

DOA Estimation with Non-Uniform Linear Arrays: A Phase-Difference Projection Approach

Hui Chen, Tarig Ballal, and Tareq Y. Al-Naffouri

Abstract—Phase wrapping is a major problem in direction-of-arrival (DOA) estimation using phase-difference observations. For an antenna pair with an inter-antenna spacing greater than half of the wavelength ($\lambda/2$) of the signal, phase wrapping occurs at certain DOA angles leading to phase-difference ambiguities. Existing phase unwrapping methods exploit either frequency or spatial diversity. These techniques work by imposing restrictions on the utilized frequencies or the receiver array geometry. In addition to these restrictions, sensitivity to noise and calibration errors is another limitation of these methods. We propose a grid-less *phase-difference projection* (PDP) DOA algorithm to overcome these issues. The concept of *wrapped phased-difference pattern* (WPDP) is introduced, which allows us to compute most of the parameters required for DOA estimation in an offline manner. This results in a superior computational speed in real-time compared to methods with similar DOA estimation performance. Simulation results demonstrate the excellent performance of the proposed algorithm, both in terms of accuracy and speed.

Index Terms—Direction of arrival, DOA, phase-difference, phase wrapping, non-uniform linear arrays, CRLB.

I. INTRODUCTION

Direction-of-arrival (DOA) estimation is an important topic for applications such as wireless sensor networks [1], indoor positioning and tracking [2], Radar [3], wireless communications [4], and so on. Many DOA estimation methods have been proposed over the years [5], [6], focusing largely on uniform linear array (ULA) configurations. On the other hand, the use of non-uniform linear arrays (NULAs) is also popular. NULA configurations are often utilized to extend the array aperture and consequently improve the array's DOA resolution.

In this paper, we focus on single-source DOA estimation with NULAs. This scenario is motivated by a mmWave/THz multiple-input multiple-output (MIMO) communication context. In these systems, flexible arrays are adopted to alleviate the high computation and hardware costs (see switch-based MIMO [7] and array-of-subarray (AOSA) structures [8]). When an antenna/subarray selection algorithm is applied, a NULA structure will be formed. In addition to the NULA structure, the analog beamforming employed in these systems can reduce multipath and provide a dominant line-of-sight (LOS) signal [9]. Hence, DOA estimation for a single source observed at a NULA is an important problem for mmWave/THz MIMO systems.

The DOA estimation problem can be formulated as an optimization of a cost function over a feasible DOA range.

The authors are with the Division of Computer, Electrical and Mathematical Science & Engineering, King Abdullah University of Science and Technology (KAUST), Thuwal, 23955-6900, KSA. e-mail: {hui.chen; tarig.ahmed; tareq.alnaffouri}@kaust.edu.sa.

Usually, the process requires evaluating the cost function for the whole DOA range, searching for that function's optimum. Maximum likelihood estimation (MLE) [10] and MUSIC [11] are two widely used methods that exemplify this approach. A drawback of this approach is that the search process can increase the computational complexity, especially when high spatial resolution is desired.

Time-delay estimation is a fast alternative solution to DOA estimation that can produce a DOA estimate directly without applying a grid search. [12]. The linear relationship between time delay and phase-difference makes it possible to utilize phase-difference measurements for DOA estimation. Phase-difference based DOA estimation has been reported as an effective approach for multi-carrier signals [13], [14]. Nevertheless, phase-difference based DOA estimation suffers from the occurrence of *phase wrapping* [15], [16].

The issue of phase wrapping can be resolved by exploiting the frequency diversity available in multi-frequency signals, or by leveraging spatial diversity in single-frequency scenarios [17]. Examples of spatial-diversity phase unwrapping methods include [15], and more recent off-grid approaches such as 2Q-order difference-set [18] and two-step offset correction [19]. A major drawback of these methods is that they require a specialized antenna setup. Besides, these methods tend to be sensitive to the phase noise effect.

This paper proposes a *phase-difference projection* (PDP) method for DOA estimation using non-uniform linear arrays. We capitalize on a novel concept of a *wrapped phased-difference pattern* (WPDP). The proposed method can be applied to an arbitrary linear array configuration of three or more sensors. Simulation results demonstrate that the proposed method offers a good trade-off between computational complexity and DOA estimation performance.

We proceed by presenting the observation model in Section II and the proposed PDP approach for DOA estimation in Section III. Simulation results are presented in Section IV before drawing the conclusion of the paper in Section V.

II. OBSERVATION MODEL

We consider a complex sinusoidal source signal, with a frequency f and amplitude A , $s(t) = Ae^{-j2\pi ft}$ in the *far field* [20] of a non-uniform linear array of N antennas. The source impinges on the array from a direction $\theta \in [-\pi/2, \pi/2]$ rad. Let d_{uv} denote the distance between a pair of the array antennas (u and v) normalized by $\lambda/2$, where λ is the signal wavelength. The received signal (vector) at time t can be modeled as [21]

$$\mathbf{x}(t) = \mathbf{a}(\theta)s(t) + \mathbf{w}(t), \quad (1)$$

arXiv:2102.03650v2 [eess.SP] 21 Oct 2021

where $\mathbf{a}(\theta) = [1, e^{-j\pi d_{12}\sin(\theta)}, \dots, e^{-j\pi d_{1N}\sin(\theta)}]^T$ is the array steering vector, $(\cdot)^T$ indicates the transpose operation, and $\mathbf{w}(t)$ is a vector of additive white Gaussian noise (AWGN).

The *wrapped phase-difference* (WPD) across an antenna pair, u and v , can be estimated from the u -th and v -th elements of \mathbf{x} as

$$\hat{\psi}_{uv}(t) = \text{angle}(x_u(t) \cdot x_v^*(t)) \in [-\pi, \pi], \quad (2)$$

where $(\cdot)^*$ is the complex conjugate operation. For simplicity, and without loss of generality, we will focus on single-snapshot scenarios. Hence, we will drop the time variable t .

To develop our proposed method, we start from noise-free WPD observations, $\psi_{uv}(\theta)$. These are related to the *actual phase-difference*, $\phi_{uv}(\theta) = \pi d_{uv} \sin(\theta)$ through

$$\psi_{uv}(\theta) = \text{mod}(\phi_{uv}(\theta) + \pi, 2\pi) - \pi = \pi d_{uv} \sin(\theta) - 2\pi q_{uv}, \quad (3)$$

where $\text{mod}(\cdot, \cdot)$ is the modulus operation. The value of q_{uv} can be obtained as

$$q_{uv} = \text{round}\left(\frac{\pi d_{uv} \sin(\theta)}{2\pi}\right), \quad (4)$$

where $\text{round}(\cdot)$ is the integer rounding operation.

Based on (3), we observe that estimating the DOA from $\psi_{uv}(\theta)$ requires knowledge of the integer q_{uv} , which is not available since we use (2) to estimate $\psi_{uv}(\theta)$. When $d_{uv} \leq 1$, $q_{uv} = 0$ for any θ . However, for $d_{uv} > 1$, the latter result is not guaranteed, except for a specific range of θ values. Since θ is unknown, $\psi_{uv}(\theta)$ will always be *ambiguous* for $d_{uv} > 1$, which is the case for most of the antenna pairs in a NULA.

III. THE PROPOSED PDP ALGORITHM

A. Wrapped Phase-Difference Pattern (WPDP)

For an arbitrary source location $\theta \in [-\pi/2, \pi/2]$, using (3), we can compute the WPD across receiver pairs to create a WPD vector $\boldsymbol{\psi}(\theta) = [\psi_{uv}(\theta)]^T$, $u, v \in \{1, \dots, N\}$, $u < v$. Assuming that we utilize $M \leq \binom{N}{2}$ antenna pairs, we can simplify the notations and write $\boldsymbol{\psi}(\theta) = [\psi_m(\theta)]^T$, and $\mathbf{q}(\theta) = [q_m(\theta)]^T$, $m = 1, \dots, M$. We can also arrange the inter-antenna distances that correspond to $\boldsymbol{\psi}(\theta)$ in a vector $\mathbf{d} = [d_m]^T$.

Now, let us think of $\boldsymbol{\psi}(\theta)$ as a point in an M -dimensional space. From (3), and for $\theta = 0$, we can see that $\psi_m(\theta) = 0$, $q_m(\theta) = 0$, $\forall m \in \{1, \dots, M\}$. By gradually increasing θ starting from $\theta = 0$, we can see that all $\psi_m(\theta)$ increase linearly with $\sin(\theta)$. The entries of the vector $\mathbf{q}(\theta)$ remain constant (all zeros) up to a certain θ value at which the entry corresponding to the largest inter-antenna spacing will have an increment of $+1$. Then, again, $\mathbf{q}(\theta)$ will remain constant until another entry changes its value. The elements of $\mathbf{q}(\theta)$ will successively change their value until we reach $\theta = \pi/2$. A similar phenomenon is observed when θ is varied in the negative direction starting from zero—the entries of $\mathbf{q}(\theta)$ successively be incremented by -1 . This process creates different intervals of θ , each interval with a distinct vector \mathbf{q} that remains unchanged throughout that interval. Let us denote these intervals as Θ_k , $k \in \{1, \dots, K\}$. For any $\theta_a, \theta_b \in \Theta_k$,

$$\mathbf{q}(\theta_a) = \mathbf{q}(\theta_b) = \mathbf{q}_k. \quad (5)$$

Based on (3) and (5), we can write

$$\delta_{ab} = \boldsymbol{\psi}(\theta_a) - \boldsymbol{\psi}(\theta_b) = \pi \mathbf{d} [\sin(\theta_a) - \sin(\theta_b)], \quad (6)$$

which indicates that each continuum given by $\boldsymbol{\psi}(\Theta_k)$, $k \in \{1, \dots, K\}$, is a straight line; and that all the K straight lines point in the same direction $\mathbf{d}/\|\mathbf{d}\|_2$, where $\|\cdot\|_2$ is the Euclidean norm. That is, we have K parallel lines in M -dimensional space, with K given by [14]

$$K = 2 \sum_{i=1}^M \text{ceil}\left(\frac{\psi_i(\pi/2) - \psi_i(-\pi/2)}{2\pi}\right) + 1, \quad (7)$$

where $\text{ceil}(\cdot)$ returns the nearest integer greater than or equal to the argument. These K lines result from *abrupt changes* in the linear relationship between the entries of the vector $\boldsymbol{\psi}(\theta)$ that occur when an entry of $\mathbf{q}(\theta)$ changes its value. We refer a plot of $\boldsymbol{\psi}(\theta)$ as a *wrapped phase-difference pattern* (WPDP).

An illustration of a WPDP for an array of 3 elements is depicted in Fig. 1. We use $M = 2$ and $\boldsymbol{\psi}(\theta) = [\psi_{12}(\theta), \psi_{23}(\theta)]^T$. The inter-antenna spacing vector is $\mathbf{r} = [0, 2.3, 5.18]$ (relative to antenna-1). We can see $K = 5$ WPD lines displayed together with the corresponding projection points, \mathbf{p}_k , $k = 1, \dots, 5$ (will be discussed shortly). These five lines represent the relationship between the entries of $\boldsymbol{\psi}(\theta)$ as θ changes (see (3)). Sample θ values (in degrees) are indicated.

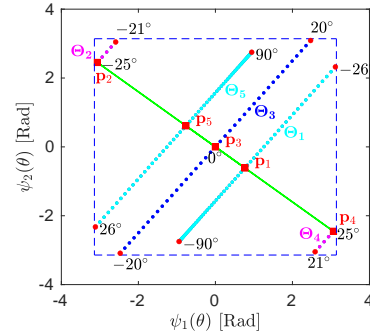


Fig. 1. An example of a WPDP for $\mathbf{r} = [0, 2.3, 5.18]$, $M = 2$.

Using simple geometry, we can see that all the WPD lines $\boldsymbol{\psi}(\Theta_k)$ (dotted lines) are perpendicular to a hyperplane (solid green line in this 2-dimensional WPDP) that contains the origin. This hyperplane is formed by the points $\boldsymbol{\psi}$ that satisfy

$$\mathbf{d}^T \boldsymbol{\psi} = d_1 \psi_1 + d_2 \psi_2 + \dots + d_M \psi_M = 0. \quad (8)$$

Each line $\boldsymbol{\psi}(\Theta_k)$ has a *projection point*, \mathbf{p}_k , at which the line intersects with the hyperplane. In the following discussion, we show how to compute these projection points.

Given a noise-free WPD vector $\boldsymbol{\psi}(\theta)$, the distance between this vector, treated as a point in M -dimensional space, and the hyperplane (8), is given by

$$\text{dist}(\boldsymbol{\psi}(\theta), \mathbf{d}^T \boldsymbol{\psi} = 0) = \frac{\mathbf{d}^T \boldsymbol{\psi}(\theta)}{\|\mathbf{d}\|_2}. \quad (9)$$

The projection point $\mathbf{p}(\theta)$ of $\boldsymbol{\psi}(\theta)$ on the hyperplane along the direction $\mathbf{d}/\|\mathbf{d}\|$ can be obtained as

$$\mathbf{p}(\theta) = \text{project}(\boldsymbol{\psi}(\theta)) = \boldsymbol{\psi}(\theta) - \frac{\mathbf{d}^T \boldsymbol{\psi}(\theta)}{\|\mathbf{d}\|_2} \cdot \frac{\mathbf{d}}{\|\mathbf{d}\|_2}. \quad (10)$$

It is obvious that all points on the same WPD line are projected on the same point in the projection hyperplane. However, for an observed noisy wrapped phase-difference vector $\hat{\psi}$, (10) returns a perturbed projection point, possibly $\hat{\mathbf{p}} \notin \{\mathbf{p}_k\}$. In this case, we pick the nearest projection point \mathbf{p}_z , where

$$z = \arg \min_k \|\mathbf{p}_k - \hat{\mathbf{p}}\|_2. \quad (11)$$

Now, the unbiased WPD $\tilde{\psi}$, which is the nearest point on the line with the projection point \mathbf{p}_k can be estimated as

$$\tilde{\psi} = \mathbf{p}_z + \frac{\mathbf{d}^T \hat{\psi}}{\|\mathbf{d}\|_2} \cdot \frac{\mathbf{d}}{\|\mathbf{d}\|_2}. \quad (12)$$

Based on (5), all points on the k -th wrapped phase-difference (WPD) line can be compensated/unwrapped with the same *unwrapping vector* $\mathbf{h}_k = 2\pi\mathbf{q}_k$, i.e., $\phi(\theta) = \psi(\theta) + \mathbf{h}_k, \forall \theta \in \Theta_k$. Hence, the estimated *unwrapped* phase difference can be obtained as

$$\hat{\phi} = \hat{\psi} + \mathbf{h}_z. \quad (13)$$

A procedure to compute the unwrapping vector \mathbf{h}_k and the projection points \mathbf{p}_k will be detailed in the next subsection.

B. Computing the Unwrapping Vectors and Projection Points

The unwrapping vector \mathbf{h}_k can be obtained by tracing the WPD lines. Together with their projection points, these lines are easily identified by their (known) direction unit vectors and starting points. We can start from the point $\psi(-\pi/2)$, which, let us say, falls on the first line. The point where this line intersects with the M-cube whose boundaries are $-\pi$ and π can easily be calculated. The intersection point determines the next line's starting point, which is obtained by wrapping the coordinate of ψ that crosses the cube's surface. A pseudocode for calculating \mathbf{p}_k and \mathbf{h}_k is listed in Algorithm 1, where ϕ_0 , ψ_0 and \mathbf{h}_0 are intermediate variables. The procedure in Algorithm 1 is performed completely offline, which reduces the online complexity of the proposed algorithm.

Algorithm 1 – Calculate $\mathbf{h}_k, \mathbf{p}_k$

- 1: $\phi_0 \leftarrow \pi\mathbf{d} \sin(-\pi/2), \phi_{max} \leftarrow \pi\mathbf{d} \sin(\pi/2)$
- 2: $j \leftarrow 1, \mathbf{h}_0 \leftarrow \phi_0 - \text{wrap}(\phi_0)$
- 3: **while** $\phi_0(m) < \phi_{max}(m)$ for all $m = [1, 2, \dots, M]$ **do**
- 4: $\mathbf{h}_j \leftarrow \mathbf{h}_0$
- 5: $\mathbf{p}_j \leftarrow \text{project}(\psi_0)$
- 6: $j \leftarrow j + 1$
- 7: $i \leftarrow \arg \min_i [(\pi - \psi_c(i))/d_i]$
- 8: $\psi_0 \leftarrow \mathbf{d}(\pi - \psi_0(i))/d_i + \psi_0$
- 9: $\psi_0(i) \leftarrow \psi_0(i) - 2\pi$
- 10: $\mathbf{h}_0(i) \leftarrow \mathbf{h}_0(i) + 2\pi$
- 11: $\phi_0 = \psi_0 + \mathbf{h}_0$
- 12: **return** $\mathbf{h}_k, \mathbf{p}_k (k \in \{1, 2, \dots, K = j - 1\})$

C. PDP DOA Estimation Algorithm

Given a noisy WPD $\hat{\psi}$, the estimated projection point $\hat{\mathbf{p}}$ can be computed using (10) and (11). Then, the unbiased WPD $\tilde{\psi}$ can be obtained using (12). Next, the estimated unwrapped

phase-difference vector $\hat{\phi}$ can be obtained using (13). Finally, the DOA of the source can be calculated using (3). A pseudocode of the proposed algorithm is listed in Algorithm 2 (Matlab codes available in *Github*).

Remark 1: In Algorithm 2, we note that the bulk of the computational complexity lies in Step-1. This step needs to be performed only once at the initial setup (offline). The rest of the algorithm's (online) steps involve simple computations. This, along with its grid-less nature, greatly enhances the online computational complexity of the proposed algorithm.

Algorithm 2 – PDP DOA Estimation Algorithm

- 1: Initialize $\mathbf{h}_1\text{-}\mathbf{h}_K, \mathbf{p}_1\text{-}\mathbf{p}_K$ using Algorithm 1
- 2: $\hat{\psi} \leftarrow \text{angle}(x_u(t_0) \cdot x_v^*(t_0))$ for selected pairs (2)
- 3: $\hat{\mathbf{p}} \leftarrow \hat{\psi} - \frac{\mathbf{d}^T \hat{\psi}}{\|\mathbf{d}\|} \cdot \frac{\mathbf{d}}{\|\mathbf{d}\|}$ (10)
- 4: $z \leftarrow \arg \min_k \|\mathbf{p}_k - \hat{\mathbf{p}}\|$ (11)
- 5: $\tilde{\psi} \leftarrow \mathbf{p}_z + \frac{\mathbf{d}^T \hat{\psi}}{\|\mathbf{d}\|} \cdot \frac{\mathbf{d}}{\|\mathbf{d}\|}$ (12)
- 6: $\hat{\phi} \leftarrow \tilde{\psi} + \mathbf{h}_z$ (13)
- 7: $\hat{\theta} \leftarrow \sin^{-1} \left(\frac{\hat{\phi}_1}{\pi d_1} \right)$ (3)
- 8: **return** $\hat{\theta}$

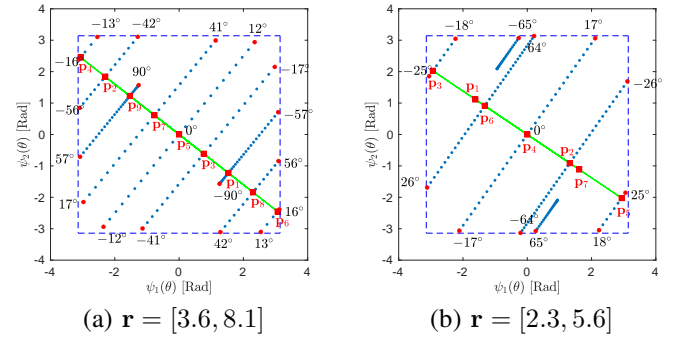


Fig. 2. Visualization of two different WPDs.

Remark 2: Noise perturbation in WPD tends to drift a noisy WPD point away from its original (noise-free) WPD line. The proposed PDP algorithm associates a noisy point with the closest projection point. Depending on the noise level, and the distance between the projection points, this might lead to a wrong (hard) decision and erroneous DOA estimation. For a specific signal frequency, the distance between the projection points is solely determined by the array layout, which can easily be deduced from (10). We illustrate the impact of array configuration in Fig. 2, which shows WPD examples for two different array configurations with the same number of elements. From the figure, we can see a significant difference in WPD structures for the two arrays, as reflected in the number of projection points and the inter-point distances. As an example, it is expected that recovering a projection point correctly from noisy observations to be easier for \mathbf{p}_4 in Fig. 2 (b) compared to the rest of the projection points in both Fig. 2 (a) and (b). On the other hand, in situations where two WPD lines overlap, the proposed algorithm, or any other DOA

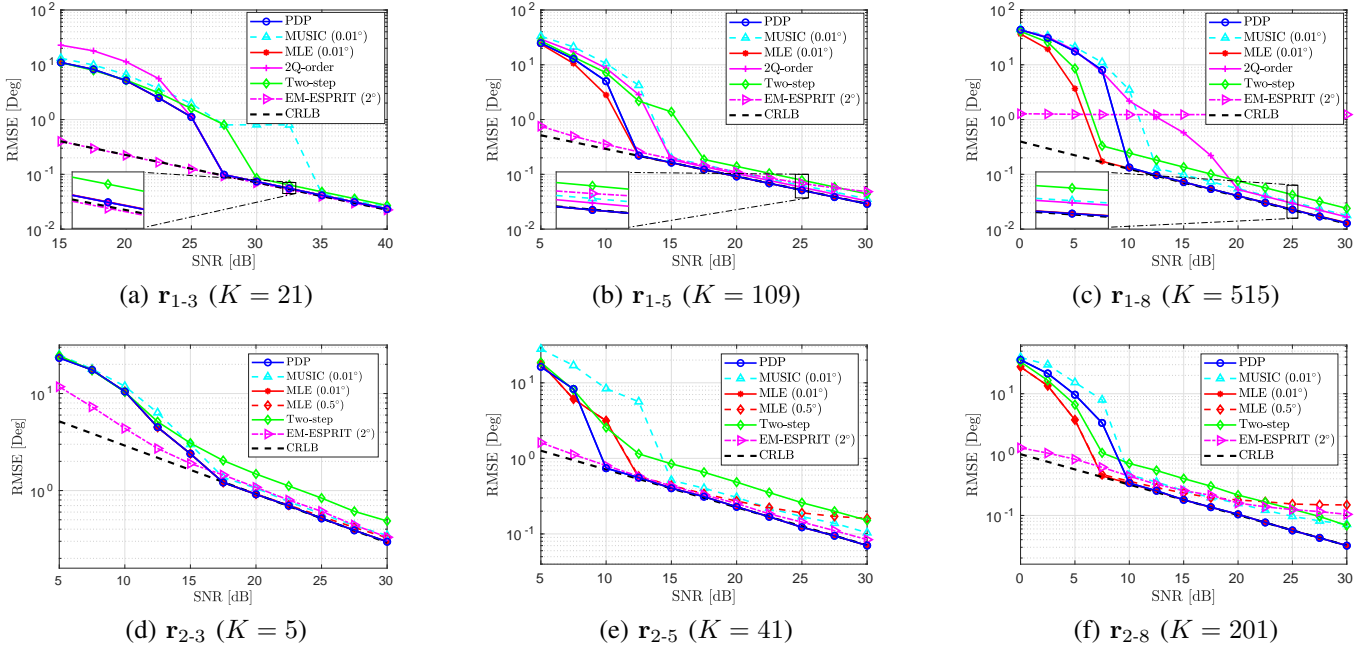


Fig. 3. RMSE versus SNR for different algorithms tested over six different array configurations. K is the number of projection points in each setup.

estimation algorithm, will fail to identify the source location. This happens when the array configuration is *ambiguous* [22].

IV. PERFORMANCE EVALUATION

In this section, we evaluate the performance of the proposed PDP algorithm given in Algorithm 2 along with several benchmark methods. The benchmark methods are the 2Q-order algorithm [18], the two-step offset correction method [19], the expectation maximization ESPRIT (EM-ESPRIT) algorithm for NULAs [23], the MUSIC algorithm [11], and the MLE [10]. We also compare with Cramér-Rao lower bound (CRLB) given by [10]

$$\text{CRLB} = \frac{1}{2\pi^2 N S U \sin(\theta)}, \quad U = \frac{1}{N} \sum_{n=1}^N (r_n - \bar{r})^2, \quad (14)$$

where θ is the source location, S is the linear signal-to-noise ratio (SNR), and \mathbf{r} is an $N \times 1$ antenna spacing vector, r_n and \bar{r} are the n -th element and the average value of \mathbf{r} , respectively.

TABLE I
ONLINE COMPUTATIONAL COMPLEXITY FOR DIFFERENT ALGORITHMS

Algorithms	Off-Grid	Number of Multiplications
PDP	Yes	$(K+6) \frac{N(N-1)}{2}$
Two-step	Yes	$(K_c+1)N$
2Q-order	Yes	N
EM-ESPRIT	Yes	$K_i(2N_v^2 + \frac{16}{5}N_v^3)$
MUSIC	No	$\frac{16}{5}N^3 + (K_c+K_f+\frac{N}{2})N(N+1)$
MLE	No	$(K_c+K_f+\frac{1}{2})N(N+1)$

A. Computational Complexity Analysis

We use the number of multiplication operations to characterize each algorithm's computational complexity, as summarized

TABLE II
ONLINE MULTIPLICATIONS REQUIRED WITH DIFFERENT CONFIGURATIONS

Algorithms	r1-3	r1-5	r1-8	r2-3	r2-5	r2-8
PDP	81	1150	14588	33	470	5796
MLE	8670	21675	52020	8670	21675	52020

in Table I. The symbol K denotes the number of projection points of the PDP algorithm, which is array-layout dependent, as given in (7). The symbols N_v and K_i are the virtual array size and the number of iterations for EM-ESPRIT. For grid-search-based methods, the parameters K_c and K_f are the numbers of grid points used in the coarse search and fine search, respectively. From the table, we observe that 2Q-order has the lowest computational cost of all algorithms, which depends only on N . However, this algorithm requires specific array configurations. The two-step method has the second-lowest complexity, which is $\propto K_c N$. For PDP, EM-ESPRIT, MUSIC, and MLE, the complexity comparison depends on the values of K , K_i , K_c , and K_f . PDP can outperform the former two algorithms in computational complexity when K is small compared to K_i and $K_c + K_f$.

B. Simulation Results

In our simulations, we utilize two array configurations, namely, $\mathbf{r}_1 = [0, 5, 10.5, 16.5, 23, 30, 37.5, 45.5]$ (setup from [18]) and $\mathbf{r}_2 = [0, 0.4, 2.4, 4, 9.2, 10.4, 13.6, 16.4]$ (a non-redundant array from [24]). From these arrays, we create six scenarios using three subarrays of each of \mathbf{r}_1 and \mathbf{r}_2 with different number of antennas $N=3, 5, 8$ (e.g., $\mathbf{r}_{1-3} = [0, 5, 10.5]$ is a subarray of the first three elements of \mathbf{r}_1). For each scenario, we plot the *root mean squared error* (RMSE) versus SNR calculated from 1000 simulation trials at each SNR value.

In each trial, the source location is generated randomly from a uniform distribution between 39.5° to 40.5° . For the proposed method, $M = \binom{N}{2}$ phase-difference estimates are computed using (2). For the MUSIC and MLE algorithms, the search is implemented in two stages [10]—a coarse search in the interval $[-70^\circ, 70^\circ]$ using a 0.2° step followed by a fine search using a 0.01° step. An initial estimation is needed for the EM-ESPRIT [23], which is chosen randomly from $[\theta - 2^\circ, \theta + 2^\circ]$. Also, we set $K_i = 20$. In all simulation trials, and for all methods, a single snapshot is used to estimate the source location. The RMSE performance for all scenarios is presented in Fig. 3. The 2Q-order algorithm only works for \mathbf{r}_1 due to a specific geometry requirement, and hence is not shown in the results based on \mathbf{r}_2 (Fig. 3 (d)-(f)).

For the scenarios of Fig. 3, the proposed PDP algorithm mostly matches the RMSE of the MLE (fine search resolution of 0.01°), with some deviations that occur at low SNRs, especially for relatively large arrays. Both PDP and MLE (0.01° resolution) achieve the CRLB at high SNRs in all the tested scenarios. The other benchmark methods tend to lack *consistency* as they deviate from the CRLB in the high SNR regime (exceptions are the 2Q-order and EM-ESPRIT algorithms in Fig. 3 (a)). The EM-ESPRIT algorithm tends to outperform the rest of the methods at low SNRs. However, this can be attributed to the extra information available to this algorithm in the form of a good initial point. The performance of the on-grid methods (MUSIC and MLE) highly depends on the search step. As an example, the MLE performance using only a (coarse) search step of 0.5° deviates from the CRLB in scenarios (e) and (f).

As for computational complexity, the two-step and 2Q-order methods require fewer computations than all the other methods. Based on the above discussion, these methods, together with MUSIC and EM-ESPRIT, offer inferior performance on average (compared to PDP and MLE). Therefore, in Table II, we show the actual number of multiplications for only PDP and MLE (with 0.01° search step) in all six scenarios. From the table, we observe a substantial advantage for the proposed PDP algorithm. This advantage is attributed mainly to the avoidance of grid search and that the proposed algorithm performs a good amount of its computations offline.

V. CONCLUSION

A phase-difference projection (PDP) direction of arrival (DOA) algorithm is proposed. The proposed algorithm projects the phase-difference observations measured across antenna pairs on a predefined hyperplane determined by the array geometry. Based on this projection, DOA estimation can be achieved in a simple and computationally efficient manner. Simulation results show that the proposed algorithm can match maximum likelihood estimation while maintaining a significant computational-complexity advantage.

REFERENCES

[1] S. Tomic, M. Beko, and R. Dinis, "3-D target localization in wireless sensor networks using RSS and AoA measurements," *IEEE Transactions on Vehicular Technology*, vol. 66, no. 4, pp. 3197–3210, 2016.

[2] L. Wan, G. Han, L. Shu, S. Chan, and T. Zhu, "The application of DOA estimation approach in patient tracking systems with high patient density," *IEEE Transactions on Industrial Informatics*, vol. 12, no. 6, pp. 2353–2364, 2016.

[3] J. Xu, W.-Q. Wang, and R. Gui, "Computational efficient DOA, DOD, and Doppler estimation algorithm for MIMO radar," *IEEE Signal Processing Letters*, vol. 26, no. 1, pp. 44–48, 2018.

[4] H. Huang, J. Yang, H. Huang, Y. Song, and G. Gui, "Deep learning for super-resolution channel estimation and DOA estimation based massive MIMO system," *IEEE Transactions on Vehicular Technology*, vol. 67, no. 9, pp. 8549–8560, 2018.

[5] H. Krim and M. Viberg, "Two decades of array signal processing research," *IEEE signal processing magazine*, 1996.

[6] T. E. Tuncer and B. Friedlander, *Classical and modern direction-of-arrival estimation*. Academic Press, 2009.

[7] S. Payami, N. M. Balasubramanya, C. Masouros, and M. Sellathurai, "Phase shifters versus switches: An energy efficiency perspective on hybrid beamforming," *IEEE Wireless Communications Letters*, vol. 8, no. 1, pp. 13–16, 2018.

[8] W. Huang, Z. Lu, Y. Huang, and L. Yang, "Hybrid precoding for single carrier wideband multi-subarray millimeter wave systems," *IEEE Wireless Communications Letters*, vol. 8, no. 2, pp. 484–487, 2018.

[9] H. Saeeddeen, M.-S. Alouini, and T. Y. Al-Naffouri, "An overview of signal processing techniques for terahertz communications," *arXiv preprint arXiv:2005.13176*, 2020.

[10] F. Athley, "Threshold region performance of maximum likelihood direction of arrival estimators," *IEEE Transactions on Signal Processing*, vol. 53, no. 4, pp. 1359–1373, 2005.

[11] R. Schmidt, "Multiple emitter location and signal parameter estimation," *IEEE transactions on antennas and propagation*, vol. 34, no. 3, pp. 276–280, 1986.

[12] L. Liu and H. Liu, "Joint estimation of DOA and TDOA of multiple reflections in mobile communications," *IEEE Access*, vol. 4, pp. 3815–3823, 2016.

[13] H. Chen, T. Ballal, and T. Y. Al-Naffouri, "Fast phase-difference-based doa estimation using random ferns," in *2018 IEEE Global Conference on Signal and Information Processing (GlobalSIP)*, 2018, pp. 256–260.

[14] H. Chen, T. Ballal, X. Liu, and T. Y. Al-Naffouri, "Realtime 2-D DOA estimation using phase-difference projection (PDP)," in *2019 27th European Signal Processing Conference (EUSIPCO)*. IEEE, 2019, pp. 1–5.

[15] T. Ballal and C. J. Bleakley, "DOA estimation of multiple sparse sources using three widely-spaced sensors," in *2009 17th European Signal Processing Conference*. IEEE, 2009, pp. 1978–1982.

[16] Molaei, Amir Masoud, and Masoud Hoseinzade, "High-performance 2D DOA estimation and 3D localization for mixed near/far-field sources using fourth-order spatiotemporal algorithm," *Digital Signal Processing*, vol. 100, p. 102696, 2020.

[17] T. Ballal and C. J. Bleakley, "DOA estimation for a multi-frequency signal using widely-spaced sensors," in *2010 18th European Signal Processing Conference*. IEEE, 2010, pp. 691–695.

[18] Y. Li, X. Zou, B. Luo, W. Pan, L. Yan, and P. Liu, "A $2q$ -order difference-set approach to eliminate phase ambiguity of a single-frequency signal," *IEEE Signal Processing Letters*, vol. 26, no. 10, pp. 1526–1530, 2019.

[19] Y. Ma, X. Cao, and X. Wang, "Off-grid doa estimation with arbitrary-spaced linear array using single snapshot," in *2019 IEEE Radar Conference (RadarConf)*. IEEE, 2019, pp. 1–6.

[20] J. R. Gonzalez and C. J. Bleakley, "High-precision robust broadband ultrasonic location and orientation estimation," *IEEE Journal of selected topics in Signal Processing*, vol. 3, no. 5, pp. 832–844, 2009.

[21] C. Zhou, Y. Gu, X. Fan, Z. Shi, G. Mao, and Y. D. Zhang, "Direction-of-arrival estimation for coprime array via virtual array interpolation," *IEEE Transactions on Signal Processing*, vol. 66, no. 22, pp. 5956–5971, 2018.

[22] A. Manikas and C. Proukakis, "Modeling and estimation of ambiguities in linear arrays," *IEEE Transactions on Signal Processing*, vol. 46, no. 8, pp. 2166–2179, 1998.

[23] C. El Kassis, J. Picheral, and C. Mokbel, "EM-ESPRIT algorithm for direction finding with nonuniform arrays," in *2007 IEEE/SP 14th Workshop on Statistical Signal Processing*. IEEE, 2007, pp. 453–457.

[24] E. Vertatschitsch and S. Haykin, "Nonredundant arrays," *Proceedings of the IEEE*, vol. 74, no. 1, pp. 217–217, 1986.